Ice-Water Phantom Localisation for Diffusion Calibration

Hossein Ragheb[1]
hossein.ragheb@manchester.ac.uk
Neil A. Thacker[2]
http://www.tina-vision.net/~nat/
David M. Morris[2]
David.M.Morris@manchester.ac.uk
Naomi H. M. Hogg[3]
Naomi.Hogg@icr.ac.uk
Alan Jackson[1]
alan.jackson@manchester.ac.uk

[1] The Wolfson Molecular Imaging Centre, Faculty of Medical and Human Sciences, University of Manchester, Manchester, UK
[2] Imaging Sciences, Faculty of Medical and Human Sciences, University of Manchester, Manchester, UK
[3] Institute of Cancer Research, Cotswold Road, Sutton, Surrey, UK

Abstract

When multiple scanners are used to acquire diffusion MR image data from the same patient, there is no guarantee that identical settings will result in comparable images of a specific organ and region. Despite this, for clinical use, any software developed to compute the apparent diffusion coefficient (ADC) must be expected to give equivalent results. What is needed is a phantom study with appropriate design which supports a calibration, so that appropriate settings for equivalent diffusion measurements can be defined among different scanners. Ideally the calibration process needs to be fully automatic, so that it can be used by non-experts in a clinical setting. We intend to develop software which automatically locates five cylinders in an ice water phantom and then measures the different diffusion values in the cylinders. The location algorithm uses an object recognition process which culminates in robust Likelihood estimation of position and orientation, computed using probabilistic Hough Transforms. This process estimates cylinder locations to an accuracy of a few pixels, even in the presence of field inhomogeneity and significant spatial distortion. Our assessment of performance includes quantification of possible errors due to; data inaccuracy, distortion due to poor shimming, signal to noise, field inhomogeneity and image clutter (i.e. ice). Results indicate that reliable localisation can be obtained using these methods for realistic clinical settings.

1 Introduction

Diffusion weighted (DW) magnetic resonance (MR) imaging has recently become a focus of attention for facilitating the diagnosis and treatment of tumors [1]. Specifically, to monitor the effect of new drugs administered to treat cancerous organs, DW-MR imaging is an attractive method compared to other alternatives including open surgery. However, there are many difficulties associated with the analysis of DW-MR images [2]. Recomendations have been made for tackling these problems, in order to ensure the validity of any corresponding

conclusions [2]. A common quantity that is used when analysing these images is the apparent diffusion coefficient (ADC). For consistency, it is important that any software developed to compute the ADC must give equivalent results on different scanners. One method to achieve this uses a non-biological phantom. For instance, Chenevert *et al*. [3] have recently performed a study using an ice-water calibration phantom and shown that it is possible to get good quantitative agreement between ADC's measured on different scanners. Gunter *et al*. [8] have used a phantom for the similar purpose of multi-centre MR (not DW-MR) scanner calibration but with a different design (and without using ice) and a different pattern recognition method.

This idea has recently been developed as part of the QUIC-CONCEPT project [1], providing us with two diffusion MR data sets. One data set corresponds to the standard shimmed scanner, while the other corresponds to a poorly shimmed scanner (Fig. 1). For diffusion measurement, image data are generally acquired at multiple b values, and exponential fits to this data generate diffusion parameters. In each data set there are five image slices for each of the four b values used (0, 100, 500 and 900), giving a total of 40 images with which to test our software. There are five cylinders of small diameter located inside the main large cylinder which is filled with ice and water. This maintains the temperature so that the measured diffusion is highly repeatable. One of the five cylinders is placed in the centre while the other four are symmetrically located around the centre (Fig. 1). Each of the five cylinders is filled with a different liquid which has specific diffusion characteristics. An automated calibration must first locate the five cylinders and the main topic of this paper is this task. We intend to use object recognition algorithms to identify and locate the phantom. However, the basic design of the phantom has 4-fold rotational symmetry, and this generates many combinatorial possibilities for location and orientation of the phantom which need to be combined and assessed. Probabilistic Hough transforms are used for this task, implemented as approximations to a likelihood estimation process, in order to deal with the large variations in the constraints on location parameters implied by the measured data.

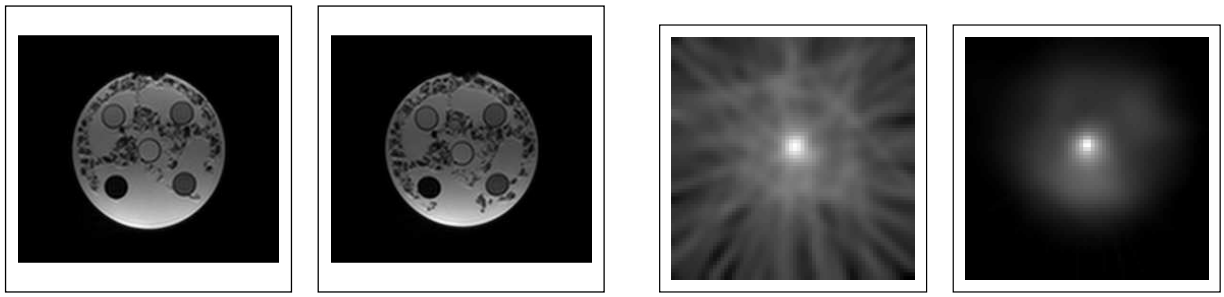

Figure 1: From left-to-right: example image slices from the standard shimmed (a) and poorly shimmed (b) phantom data; there are five different liquids with different diffusion characteristics inside the five cylinders, with ice and water at 0° temperature around them (ice appears as black irregularities); $L(x,y)$ for the standard (c) and $H(x,y)$ for the tuple Hough transfroms (d).

The combined process is expected to generate accurate estimates of phantom position even in the presence of image features such as inhomogeneity and ice, as well as being robust to significant spatial distortion and poor SNR. These issues are expected to compromise approaches based upon direct grey-level image matching and iterative optimisation.

[1]The QUIC-CONCEPT project has received funding from the European Union for the Innovative Medicine Initiative.

2 Methods and Results

We require a strategy to locate pixels falling inside each of the five cylinders in order to measure the diffusion of the liquid inside each. In our software, developed for this purpose, edge data is first extracted from the image and linked into extended curves. These curves are then approximated by polygonal approximations for convenience [4]. Each line in the polygonal description is then used as the focus for construction of a geometric histogram [5]. Geometric histograms are two dimensional and encode relative orientation and perpendicular distance between lines convolved with a PSF (point spread function) at a scale consistent with these measurements. The histograms can therefore be considered as density estimates of geometric co-occurrence. There are alternative versions of this basic representation which embody varying degrees of invariance. For the current work we used the most discriminative (least invariant) histogram, which considers two possible directions for each scene line separately, in order to compute a full 2π relative orientation. Two histograms are generated for each scene line over a range of possible scales.

The full set of histograms for all lines in the image are matched to a database of similar histograms generated using the model on the basis of a Bhattacharrya overlap [7]. The best match score and scale for each line is interpolated, so that each candidate match provides a constraint on the location, orientation and scale of the phantom in the image. The list of N best candidate matches for each scaled scene line is used as the basis for a series of probabilistic Hough transforms, which compute the robust log likelihood of centre, scale and orientation for the phantom. The 4-fold rotational symmetry of the phantom requires that $N >= 4$, and so we have used a value of $N = 8$ to guarantee that the histograms with high scores which are passed to the hough transform include the correct histogram. Likelihoods are computed on the basis of a perturbation model for the polygonalisation process, which assumes that errors on lines can be modelled using a constant uniform spherical error distribution σ_p on the end points [6]. These errors are propagated through to the parameter spaces in order to compute the required Hough entry distributions. The error model assumption is checked and the over-all scale of the spherical error determined using corresponding chi-squared distributions in data. A localisation error model with $\sigma_p = 2$ pixels was found to be approximately the correct value for this data.

Orientation and scale Hough transforms are computed as 1D histograms. The location Hough transform is 2D and entries are made for pairs of matched scene lines (n,m), i.e. a tuple Hough transform. For Gaussian density functions, the equivalent probabilistic form for this Hough transform $H(x,y)$ used to find the centroid of the phantom is given by

$$H(x,y) = \sum_m \sum_n log[p(x,y|n)p(x,y|m)] = \sum_m log[p(x,y|m)] \sum_n log[p(x,y|n)]$$

so that the total Hough entry can be considered as the square of the log Likelihood (i.e. standard Hough transform)

$$H(x,y) = L(x,y)^2 = (\sum_m log[p(x,y|m)])^2$$

In practice the 2D Gaussian distribution $p(x,y|n,m) = p(x,y|n)p(x,y|m)$ is computed directly using error propagation and then truncated at 3 S.D. to form a robust kernel. In comparison to the conventional Hough transform, the tuple based construction helps to remove background from the Hough array (Fig. 1). Cuts are placed on the allowable accuracy of each

pairwise constraint, as well as relative orientation at 5 S.D. of the propagated uncertainty in order to improve computational efficiency and further reduce background entries.

Estimated location, orientation and scale are the result of a global search of the parameter space (followed by a quadratic peak fit), thereby avoiding issues associated with local minima. These parameters are then available to project the model into the image in order to predict the location of each cylinder.

2.1 Evaluation of Cylinder Localisation

As a simple approach, we assess how well our algorithms can locate the cylinders for all image slices provided across all b values (40 images in total). This can be done by measuring the largest pixel shift between predicted and observed cylinder edges. Once this value is known it is possible to predict the quantity of usable pixels which might be reliably found in a circle around the predicted cylinder centre. Pixels falling inside these circles, may then be used to compute an average diffusion measurement. Fig. 2 shows the model overlayed on the image slices of Fig. 1. Here for the standard shimmed phantom a good match is achieved while for the poorly shimmed there is a slight mis-match. Here, it is clear that there is a systematic clockwise rotation of the model relative to the data. As the centroid of the phantom is easily estimated, the main localisation error for undistorted image geometry is generally of this nature, allowing us to attribute a sign (clockwise or anti-clockwise) to the residual error.

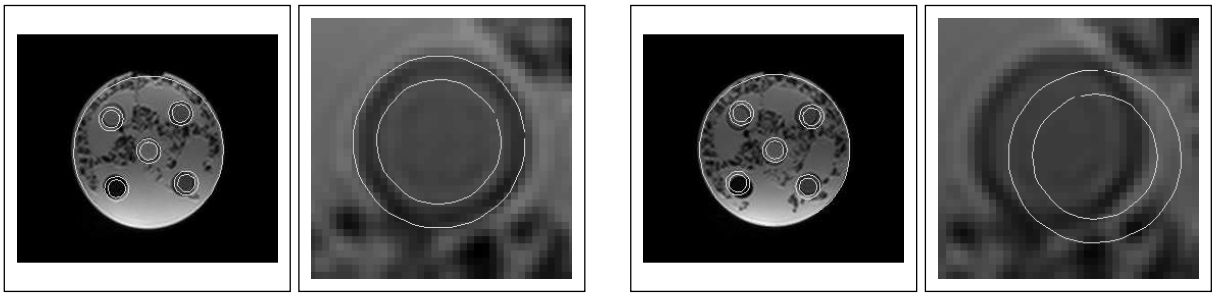

Figure 2: Locating all cylinders on image slices from standard shimmed (left) and poorly shimmed (right) data (Fig. 1) using our software; the display window is shown before and after zooming in to count the maximum out-of-fit pixels; the main error in localisation is generally in the form of a rotation; the maximum observable rotation error can be given a sign (positive if clockwise) in order to help identify systematic rotations across multiple images.

Tabulated results in Table 1 show that the mean shift of the model is comparable for both data sets, though there is evidence of a systematic rotation for the poorly shimmed data, due to significant systematic spatial distortion (columns 2-3). In both cases however, the mean maximum observed shift is ≈ 3.5 pixels for an internal cylinder diameter of 18 pixels (i.e. 20%). This error does not seem to come from problems of statistical stability (which is expected to be much better than one pixel), but rather spatial distortion of the original image. However, this does not mean that the achieved fit is distortion limited as there is also slight error on rotation due to noise and ice clutter.

In Table 1 (columns 4-5), we also list the percentage of field inhomogeneity based on the maximum coil correction together with the mean (first number) and the standard deviation (second number) for same image slices of different b values (every four rows). The degree of this inhomogeneity is substantial (a factor of two across the phantom) but does not appear to produce significant localisation errors. This is expected as the localisation is based

upon edges not absolute grey-level values. Further, in Table 1 (columns 6-7), we tabulate the percentage of ice in each image slice. These values are computed from the $b = 900$, via a manually controlled thresholding process following inhomogeneity correction, to an accuracy of around 5%. These typical percentages show that there is no observable correlation between the amount of ice and the inaccuracies seen in model matching (columns 2-3). We notice that these percentages are slightly larger for the case of poorly shimmed images.

image slices(b)	shift std	shift por	inhomogeneity (std)%	inhomogeneity (por)%	ice std%	ice por%	SNR std%	SNR por%
01(0)	+2	+3	100	140			1.45	1.76
06(100)	+2	+2	142	129			1.69	1.75
11(500)	+3	+4	125	137			1.41	1.66
16(900)	+2	+2	100	120	51.8	60.1	1.58	1.96
			116.7; 20.54	131.5; 8.96				
02(0)	-1	+2	100	143			1.66	1.93
07(100)	+4	+3	108	121			1.47	1.79
12(500)	+2	+2	100	100			1.59	1.75
17(900)	+3	+2	100	120	54.6	61.9	1.69	2.01
			102; 4.0	121; 17.57				
03(0)	+5	+2	76	106			1.70	2.20
08(100)	+2	+4	125	114			1.74	2.39
13(500)	-3	+4	100	100			1.67	2.00
18(900)	+1	+5	80	120	52.9	63.0	1.73	2.03
			95.25; 22.44	110; 8.79				
04(0)	+3	+2	114	120			1.81	1.98
09(100)	+3	+2	93	93			1.59	1.98
14(500)	-3	+4	78	80			1.74	2.27
19(900)	+3	+1	80	83	55.2	65.3	1.87	1.94
			91.25; 16.56	94; 18.2				
05(0)	-2	+3	100	100			1.81	2.20
10(100)	-2	+2	80	87			1.66	1.80
15(500)	+4	+2	78	80			1.83	1.95
20(900)	-3	+1	80	100	63.6	65.8	1.93	2.07
			84.5; 10.38	91.75; 9.94				

Table 1: Results are listed for both the standard shimmed (std) and poorly shimmed (por) image data sets; in columns 2-3 the positive sign for the number of pixels corresponds to the clockwise rotation while the negative sign corresponds to the anti-clockwise rotation; see text for further details.

Finally, in Table 1 (columns 8-9), we list the percentage of signal to noise ratios (SNR). Each ratio is computed from the distribution of second derivatives (for x and y) around zero, in a central rectangular region including all five cylinders, following coil correction. It is clear from the table that the SNR percentages are larger for the case of poorly shimmed data. However, it can be seen that for different b values the SNR changes by amounts which are small compared to measurement accuracy. Consequently, this level of noise is not large enough to test the robustness of the software to poor SNR. Hence, we selected an image with 50% ice and low geometrical distortion and added extra random noise until the software failed to locate the cylinders (where the midpoint of the predicted circles lies outside the

required liquid). It was found that for a factor of 2.5× more noise there is no observable degradation in performance, while the localisation algorithm fails 50% of the time at 3.4×, at which point the edge detector begins to fail to extract phantom structure. These noise levels are well beyond the expected levels for phantom data, consequently poor SNR is not expected to play a large part in the failure of localisation.

3 Conclusions

Our results suggest that the edge-based localisation method we have developed is robust to the main issues determining phantom data quality, such as field inhomogeneity, ice and SNR. In order to stay within the same range of image quality as seen in our tests we recommend that the quantity of ice is not allowed to rise above 70% and the SNR in the water to be kept above 5%. We have seen no evidence that the localisation process will not find the phantom in the 40 images provided with the standard parameters used for testing. Since there are five image slices per b value, it would be possible to check which of the five centres statistically agree (majority vote) in order to remove occasional localisation failures.

Future work now requires us to address two main issues. The main cause of localisation error is the spatial distortion which arises due to poor shimming. This cannot be accommodated by a localisation algorithm which assumes a rigid phantom model and implies that something must be done to accommodate slight shifts during the estimation of diffusion parameters. Also, the current algorithms localise the phantom with a 4-fold rotational ambiguity, due to the symmetry of the phantom. An additional marker has now been added to the phantom which we intend to use to select the correct rotation and as a quality check on predicted location.

References

[1] B. Turkbey, O. Aras, N. Karabulut, *et al*., Diffusion-Weighted MRI for Detecting and Monitoring Cancer: A Review of Current Applications in Body Imaging, *Diagnostic Interventional Radiology, Turkish Society of Raiology*, 18(1):46-59, 2012.

[2] A.R. Padhani, G. Liu, D. Mu-Koh, *et al*., Diffusion-Weighted Magnetic Resonance Imaging as a Cancer Biomarker: Consensus and Recommendations, *Neoplasia*, 11(2):102-125, 2009.

[3] T.L. Chenevert, C.J. Galban, M.K. Ivancevic, *et al*., Diffusion Coefficient Measurement Using a Temperature-Controlled Fluid for Quality Control in Multicenter Studies, *J. Magnetic Resonance Imaging*, 34:983-987, 2011.

[4] D.G. Lowe, Three-Dimensional Object Recognition from Two-dimensional Images, *Artificial Intelligence*, 31(3):355-395, 1987.

[5] A.C. Evans, N.A. Thacker and J.E.W. Mayhew, The Use of Geometric Histograms for Model-Based Object Recognition, *Proc. British Machine Vision Conference*, 429-438, 1993.

[6] A.P. Ashbrook, N.A. Thacker, P.I. Rockett and C.I. Brown, Robust Recognition of Scaled Shapes using Pairwise Geometric Histograms, *Proc. British Machine Vision Conference*, 503-512, 1995.

[7] N. A. Thacker, F. Ahearne and P. I. Rockett, The Bhattacharyya Metric as an Absolute Similarity Measure for Frequency Coded Data, *Kybernetika*, 34(4):363-368, 1997.

[8] J. L. Gunter, M. A. Bernstein, B. J. Borowski, *et al*. Measurement of MRI Scanner Performance with the ADNI Phantom, *MEDICAL PHYSICS*, 36(7):2193-2205, 2009.